Time-Domain Macromodel of Planar Microwave Devices by FDTD and Moment Expansion

Gaetano Marrocco, *Member, IEEE,* and Fernando Bardati, *Member, IEEE*

***Abstract*—The microwave design of highly complex systems can be addressed by segmentation techniques. To this purpose, a subsystem macromodel, such as the impulse response matrix, needs to be computed in an accurate and efficient way. In this paper, we present a combined procedure, based on finite-difference time-domain and a moment-expansion deconvolution by which the impulse response matrix is obtained via time-domain processing only. The algorithm has been tested on microwave planar devices with satisfactory accuracy.**

***Index Terms*—Deconvolution, FDTD, microwave circuits, transient response.**

I. Introduction

MODERN design of complex microwave or electronic systems, such as satellite internal circuitry and computer motherboards, requires an accurate time-domain electromagnetic analysis of the whole distributed structure. High-speed analog and digital devices, such as planar filters, couplers, impedance transformers, and integrated antennas have to be represented in detail to correctly predict and optimize the performances of the overall system. However, finite CPU resources limit the application of the conventional full-wave integral and differential methods to the analysis and optimization of small structures. Furthermore, instabilities and accuracy loss are experienced by such methods for large domains.

Recently, time-domain segmentation techniques have been proposed [1], [2] such that a complex and large structure is segmented into a set of smaller multiport electromagnetic subsystems. Each resulting module is individually simulated by an appropriate full-wave method, then a suitable definition of equivalent port voltages and currents is introduced, and finally, a compact time-domain macromodel is obtained in the form of the impulse response matrix. The whole structure is, therefore, analyzed as a composition of such macromodels, where appropriate interfaces perform the convolutions of individual responses. According to a different approach, an equivalent lumped circuit can be derived [3], [4] from each computed impulse response, and finally, data obtained via electromagnetic-field analysis can be integrated into time-domain circuital simulators such as SPICE or TOUCHSTONE [5]. The accurate computation of the impulse response of a microwave device can, therefore, play a very important role in the analysis of a composite structure.

Among available full-wave techniques, the finite-difference time-domain (FDTD) method [6] has been proven to be an efficient and accurate tool for the modeling of microwave devices such as planar structures with discontinuities [7], leaky wave antennas [8] with launchers, picosecond photoconductive switches, and interconnects in high-speed digital circuits [9]. Moreover, by local modification of the standard Yee algorithm, lumped linear and nonlinear elements can be easily included in a model [10].

In a previous paper [11], the authors presented the basic idea and the preliminary results of a new time-domain combined procedure, based on FDTD and numerical deconvolution, for the retrieval of a planar microwave device impulse response. The deconvolution was performed by a moment expansion (ME) of the input spectrum, then the impulse response was obtained in the form of a time series, whose coefficients depend on the input waveform.

In this paper, the proposed algorithm is fully described and deconvolution coefficients are obtained for two time-dependent excitations more frequently used in FDTD computations. Emphasis is devoted to the achievable accuracy and to define a rule for a suitable choice of the truncation order. In Section II, we shall give both a definition of input and output observables for multiport devices, and a review of most common excitations for FDTD computations. Section III introduces the deconvolution algorithm. Section IV presents some considerations about accuracy and numerical complexity. Finally, in Section V, examples are given for one- (patch antenna) and two-port (a planar low-pass filter) devices, showing the practicability of the method.

II. Statement of the Problem

Consider a multiport microwave device. At each port, input and output electric observables can be a physical current on a wire, a voltage drop across a couple of terminals, or inward/outward traveling-wave amplitudes.

Let $x_m(t)$ be a band-unlimited (time-dependent) excitation at the mth port and $y_n(t)$ be the output waveform at the nth port. If the device is causal, passive, and governed by linear differential equations with constant coefficients, the following convolution integral holds:

$$y_n(t) = \int_0^t h_{mn}(t-\tau)x_m(\tau)\,d\tau = h_{mn}(t) * x_m(t) \quad (1)$$

Manuscript received September 17, 1999. This work was supported in part by the Ministero dell'Università e della Ricerca Scientifica under Grant PRIN 97 and by the Agenzia Spaziale Italiana.

The authors are with the Dipartimento di Informatica Sistemi e Produzione, Università di Roma "Tor Vergata," 00133 Rome, Italy (e-mail: marrocco@disp.uniroma2.it).

Publisher Item Identifier S 0018-9480(01)05043-8.

where $h_{mn}(t)$ is the impulse response between the mth and nth ports. $h_{mn}(t)$ can be formally defined as

$$h_{mn}(t) = \mathcal{F}^{-1}\left[\frac{Y_n(\omega)}{X_m(\omega)}\right] \tag{2}$$

where $\mathcal{F}^{-1}$ is the inverse Fourier transform, $X_m(\omega) = \mathcal{F}[x_m(t)]$, and $Y_n(\omega) = \mathcal{F}[y_n(t)]$. If the FDTD method is used, the discrete Fourier transforms of $x_m(t)$ and $y_n(t)$ are performed on data sampled at time $p\Delta t$, where Δt is the time step.

According to (2), the impulse response can be obtained by frequency-domain manipulation and Fourier processing. Otherwise, it can be computed directly in the time domain by solving the integral equation (1) after time-domain discretization. In either case, the accuracy of the impulse-response computation depends on the deconvolution scheme (it will be examined in Section III) as well as on: 1) numerical noise of FDTD results; 2) FDTD finite bandwidth; and 3) input signal waveform. These three points are discussed in detail as follows.

1) Numerical noise is mainly caused by numerical dispersion [12], boundary staircasing [13], numerical approximation of differential operators, and imperfect grid termination [14]. An error of 1%–5% is normally accepted in the field computation by FDTD simulations.
2) Since the FDTD method works with an approximation of the electromagnetic boundary value problem, the computation of $Y_n(\omega)$ loses accuracy outside a frequency band $B_m = [\omega_{\min}^{\mathrm{FDTD}}, \omega_{\max}^{\mathrm{FDTD}}]$. It is known that the upper frequency depends on spatial discretization since, for a rectangular grid with largest cell size Δ, the shortest wavelength, which can be accurately resolved, is such that $\lambda_{\min} \geq n\Delta$ with $n = 8 - 10$ and, therefore, $\omega_{\max}^{\mathrm{FDTD}} = 2\pi c/(n\Delta)$, where c is the speed of light in the medium with the highest permittivity. A lower bound of the FDTD bandwidth exists since, to accurately account for slow field oscillations, the computation should be carried on for a large number of iterations, but the numerical noise limits the overall time window. Though generally not quantifiable, $\omega_{\min}^{\mathrm{FDTD}}$ is usually one or two orders of magnitude lower than $\omega_{\max}^{\mathrm{FDTD}}$. FDTD off-band noise can be reduced by bandpass filtering of the computation outcomes.
3) The input waveform for the FDTD computation must be properly chosen in order to extract the maximum information in the band of the numerical algorithm by considering that the noise on $Y_n(\omega)$ is amplified by $1/X_m(\omega)$ depending on frequency, unless $x_m(t)$ is a Dirac pulse.

Generally, smooth and narrow pulses [6] such as the Gaussian $x_G(t)$ or derivated Gaussian $x_{DG}(t)$ pulses are appropriate FDTD excitations

$$x_G(t) = e^{-((t-\tau)^2/2T^2)} \tag{3a}$$

$$x_{DG}(t) = -\frac{t-\tau}{T}e^{-((t-\tau)^2/2T^2)}. \tag{3b}$$

It is possible to set up the desired time- and frequency-domain signal features by selecting the parameters T, τ. The Gaussian pulse (3a) has a dc peak of spectral energy density. As a consequence, an important amount of energy is wasted on the excitation of spectral components of $Y(\omega)$ outside the finite bandwidth of the FDTD algorithm. The derivated Gaussian pulse (3b) diverts a little energy to low frequencies and exhibits two oscillations only. The 10% amplitude bandwidth [6] is $[0, \sqrt{\ln 100}(1/T)]$ for the Gaussian pulse and $[0.06(1/T), 2.8(1/T)]$ for the derivated Gaussian pulse. Therefore, the response, provided by FDTD for the above excitations, is band limited. Its upper frequency will be the lower one between that of the input signal and $\omega_{\max}^{\mathrm{FDTD}}$. Generally, the input signal upper frequency is lower than $\omega_{\max}^{\mathrm{FDTD}}$ in order not to excite frequency components outside the FDTD band. As a consequence, any distributed microwave device, although it is generally band unlimited, will be modeled as band limited.

III. Deconvolution by ME

Stable algorithms [15], [16] are available to solve general deconvolution problems with both discrete and continuous data without direct use of (2). However, for input waveforms, as in (3), the impulse response can be accurately approximated by a simple formula involving pure time-domain operations. For this purpose, the ME method can be applied in the form introduced by Papoulis [17] for image restoration and here extended to the specific application. Papoulis' algorithm applies when $x_m(t)$ has short duration, as compared with $y_n(t)$. This generally applies when Gaussian or derivated Gaussian waveforms are used.

The following expansion in powers of $(-j\omega)$ is considered:

$$\frac{1}{X_m(\omega)e^{j\omega t_0}} \approx \sum_{\ell=0}^{N} \frac{a_\ell}{\ell!}(-j\omega)^\ell \tag{4}$$

where the shift parameter $t_0 > 0$ must be chosen, as explained later, in order to put the center of gravity of the input signal at $t = 0$; $\{a_\ell\}$ are coefficients depending on $x(t)$. The expansion in (4) is truncated at the Nth term, where N will be referred to as the ME order.

Once the coefficients $\{a_\ell\}$ have been found for a given input, a time-domain expression for $h_{mn}(t - t_0)$ is obtained from (2) as

$$h_{mn}(t - t_0) \approx \sum_{\ell=0}^{N} \frac{a_\ell}{\ell!}\mathcal{F}^{-1}\Big[(-j\omega)^\ell Y_n(\omega)\Big]. \tag{5}$$

The deconvolution coefficients $\{a_\ell\}$ can be obtained according to a moment-matching procedure by performing a Taylor expansion of $X(\omega)e^{j\omega t_0}$, whose moments $\{\mu_k\}$ can be computed as

$$\begin{aligned}\mu_k &= \int_{-\infty}^{+\infty}(t - t_0)^k x_m(t)\,dt \\ &= \sum_{p=0}^{k}\binom{k}{p}(-t_0)^{k-p}(j)^p X_m^{(p)}(0).\end{aligned} \tag{6}$$

TABLE I
DECONVOLUTION COEFFICIENTS FOR INPUT SIGNAL $x(t)$

	non-zero average $x(t)$	zero average $x(t)$
a_0	$\frac{1}{\mu_0}$	$\frac{1}{\mu_1}$
a_1	0	0
a_2	$-\frac{\mu_2}{\mu_0^2}$	$-\frac{\mu_3}{3\mu_1}$
a_3	$-\frac{\mu_3}{\mu_0^2}$	0
a_4	$-\frac{\mu_4}{\mu_0^2}+\frac{6\mu_2^2}{\mu_0^3}$	$\frac{2\mu_3^2}{3\mu_1^3}$

The coefficients $\{a_\ell\}$ are obtained, in terms of moments $\{\mu_k\}$ by separately zeroing the coefficient of each power of ω in the following identity:

$$\left[\sum_{\ell=0}^{N}\frac{a_\ell}{\ell!}(-j\omega)^\ell\right]\cdot\left[\sum_{k=0}^{N}\frac{\mu_k}{k!}(-j\omega)^k\right]-1=0. \tag{7}$$

In Table I, the dependence of a_ℓ on μ_k is made explicit for $\ell=0,\ldots,4$ and input signal with nonzero or zero average. In these cases, the shift parameter is defined as $t_0=jX^{(1)}(0)/X(0)$ and $t_0=jX^{(2)}(0)/X^{(1)}(0)$, respectively.

Finally, it can be easily demonstrated that the impulse response may be written as

$$h_{mn}(t)\approx\begin{cases}\left[a_0\displaystyle\int_0^{t+t_0}d\tau+\sum_{k=2}^{N}\frac{a_k}{k!}\frac{d^{k-1}}{dt^{k-1}}\right]y_n(t+t_0)\\ \left[a_0+\displaystyle\sum_{k=2}^{N}\frac{a_k}{k!}\frac{d^k}{dt^k}\right]y_n(t+t_0)\end{cases} \tag{8}$$

when $x_m(t)$ has a zero (upper line) or nonzero (lower line) mean, respectively.

For application to a discrete output signal, as computed by the FDTD method, the differential operators are approximated by central differences. It is interesting to note that, according to (8), the value of $h_{mn}(\tilde{t})$, at time $t=\tilde{t}$, depends on the knowledge of $y_n(\tilde{t}+t_0)$ only in a neighborhood of $\tilde{t}$, whereas in the direct/inverse Fourier analysis, values of $y_n(t)$ on the entire axis are used. Therefore, the impulse response can be extracted from a portion of the output signal.

The expansions in (8) are rapidly convergent [17]. However, the numerical differentiation of discrete data is more and more inaccurate with the increase of the differentiation order. Therefore, only a few terms can be retained for reasonable accuracy. A second-order truncation (hereafter referred to as ME^2) was suggested in [17]. However, a fourth order truncation (ME^4) has been successfully used in this paper for Gaussian and derivated Gaussian excitations. Accordingly, the first nonzero moments are reported in Table II. Due to signal symmetries with respect to their centers of gravity, only even coefficients are present.

TABLE II
DECONVOLUTION MOMENTS FOR GAUSSIAN AND DERIVATED GAUSSIAN WAVEFORMS

	Gaussian pulse	derivated Gaussian pulse
a_0	$\frac{1}{\sqrt{2\pi}T}$	$\frac{1}{\sqrt{2\pi}T^2e^{1/2}}$
a_2	$-a_0T^2$	$-a_0T^2$
a_4	$3a_0T^4$	$6a_0T^4$

For time-domain discretization as $t=p\Delta t$, with Δt being the time step, the central difference computation of the derivatives in (8) yields

$$\begin{aligned}h_{mn}(p)&=\frac{a_4}{24\Delta t^4}\Big[y_n(p+2+p_0)+y_n(p-2+p_0)\Big]\\&+\left(\frac{a_2}{2\Delta t^2}-\frac{a_4}{6\Delta t^4}\right)\Big[y_n(p+1+p_0)+y_n(p-1+p_0)\Big]\\&+\left(a_0-\frac{a_2}{\Delta t^2}+\frac{a_4}{4\Delta t^4}\right)y_n(p+p_0)\end{aligned} \tag{9}$$

for the Gaussian pulse and

$$\begin{aligned}h_{mn}(p)&=a_0\Delta t\sum_{k=0}^{p+p_0}y_n(k+p_0)+\frac{a_4}{48\Delta t^3}\\&\cdot\Big[y_n(p+2+p_0)-y(p-2+p_0)\Big]+\left(\frac{a_2}{4\Delta t}-\frac{a_4}{24\Delta t^3}\right)\\&\cdot\Big[y_n(p+1+p_0)-y_n(p-1+p_0)\Big]\end{aligned} \tag{10}$$

for the derivated Gaussian pulse, where $p_0=int(t_0/\Delta t)$.

IV. ME VERSUS FOURIER DECONVOLUTION

Some features of the proposed deconvolution based on the ME, i.e., numerical accuracy and computational efficiency, will now be compared with those of the standard Fourier deconvolution.

A. Accuracy

Being based on a Taylor expansion, at $\omega=0$, of the input signal spectrum, the ME deconvolutions (8) behave as low-pass filters whose bandwidths depend on those of both the input and response signals, and on the truncation order of the series expansion. Therefore, it is expected that a large error is inherently associated with the deconvolution algorithm at the early transient while decreasing to the late transient.

The accuracy of ME deconvolutions has been investigated in the past on the basis of numerical examples [18]. Here, we will examine time and frequency waveforms for a simple lumped circuit in order to discuss the impulse response recovery without the errors and artifacts of numerical solutions such as those provided by the FDTD method and reviewed in Section II.

The formulas in Section III can be usefully applied to the impulse response computation if the expansion in (8) converges

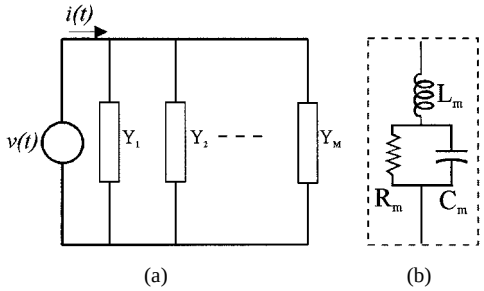

Fig. 1. (a) M-bipole lumped network. (b) Single *RLC* bipole.

TABLE III
LUMPED-NETWORK PARAMETERS

m	$R_m(\Omega)$	$L_m(pH)$	$C_m(nF)$
1	0.10	0.56	5.00
2	0.30	0.56	0.55
3	0.50	0.56	0.20
4	0.30	0.24	0.24

rapidly. This is the case if the response takes significant values [17] only in a finite range of frequencies $\omega \leq \omega_M$. Therefore, an *RLC* network consisting of the parallel connection of a finite number M of bipoles is considered (Fig. 1) as a suitable test case. Its impulse response $h(t)$ is defined as the inverse Fourier transform of the input admittance. It is easy to show that, under the constraint $R_m > \sqrt{L_m/(4C_m)}$, the impulse response of the circuit in Fig. 1 is

$$h(t) = \sum_{m=1}^{M} e^{-\gamma_m t}\Big(A_m \cos(\omega_m t) + B_m \sin(\omega_m t)\Big) \quad (11)$$

where $A_m = 1/L_m$, $B_m = (2\omega_m R_m L_m C_m)^{-1}$, $\gamma_m = (2R_m C_m)^{-1}$, and $\omega_m = \sqrt{(L_m C_m)^{-1} - (2R_m C_m)^{-2}}$.

The stimulus is a Gaussian pulse voltage $v(t)$, as in (3a). Its upper (10% amplitude) frequency $\omega_G = \ln\sqrt{100}/T$ is tuned to the 10% amplitude upper frequency of the impulse response ω_M according to $\omega_G = r\omega_M$ by selecting the parameter $r \geq 0$. The parameter τ of the Gaussian pulse is such that $v(0) = 10^{-7}v(\tau)$. For each input voltage and the corresponding network response $y(t)$, which is computed by convolution, the time response is retrieved by the ME deconvolution (h_r^N) with second- and fourth-order truncation and by Fourier deconvolution (h_r^{FFT}). The notation $h_r^N(t)$ memorizes the Gaussian input bandwidth ($r\omega_M$) and the truncation order ($N = 2$ or 4). The relative root-mean-square (rms) error is defined as

$$\delta\left(h, h_r^N\right) = \frac{\left\|h(t) - h_r^N(t)\right\|_2}{\|h(t)\|_2} \cdot 100 \quad (12)$$

where $\|h(t)\|_2 = \sum_{p=0}^{N_s}[h(p\Delta t)]^2$.

In the following numerical example, the circuit parameters are such that the resonance frequencies ω_m of the *RLC* circuit are equally spaced on the frequency axis and the damping factors γ_m grow linearly with m. The circuit parameters, for $M = 4$, are reported in Table III. For this choice, the 10% amplitude upper angular frequency is $\omega_M = 28 \cdot 2\pi$ GHz.

The spectra of the input voltage, when r takes values from 0.4 to 2, superimposed on the impulse response spectrum, are shown in Fig. 2. The response is a vector of $N_s = 2^{13}$ time samples, with time step $\Delta t = 0.6$ ns. Note that the response signal is fully damped at time $N_s\Delta t$ (overall time window).

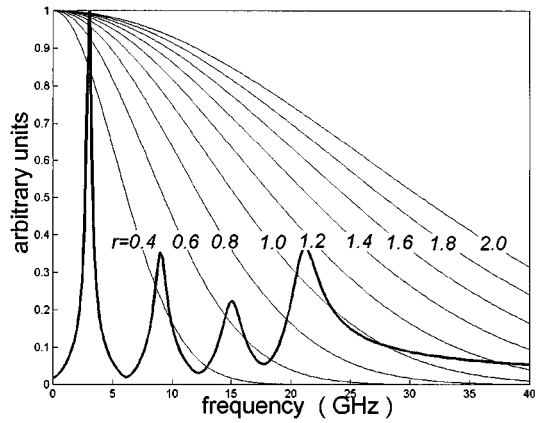

Fig. 2. Normalized spectra of the network impulse response (thick line) and of the input voltages (thin lines) for different test-signal bandwidth $\omega_G = r\omega_M$.

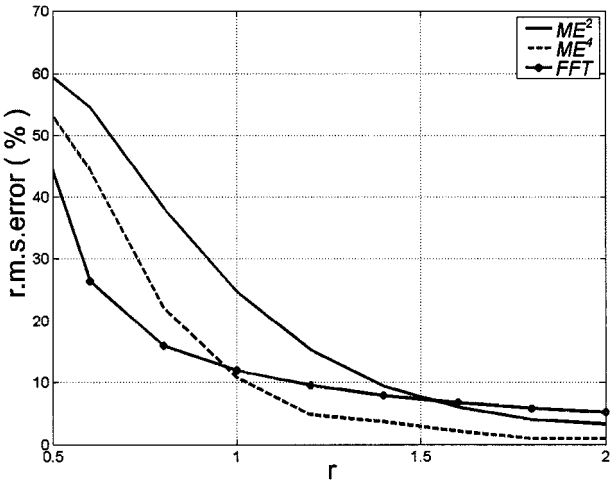

Fig. 3. rms error for ME and Fourier deconvolutions and the circuit in Fig. 1 as a function of Gaussian-pulse bandwidth $\omega_G = r\omega_M$.

Diagrams of the rms error are shown in Fig. 3 versus the input bandwidth. The error always decreases for increasing r, while it becomes less than 10% for $r > 1 - 1.5$. However, better results are obtained by fourth-order ME^4 deconvolution, than by fast Fourier transform (FFT) deconvolution (for errors less than 10%). In particular, in the case of $\omega_G = 1.5\,\omega_M$, $\delta(h, h_{1.5}^{\mathrm{FFT}}) = 7.5\%$, $\delta(h, h_{1.5}^2) = 7.7\%$, and $\delta(h, h_{1.5}^4) = 2.9\%$. The retrieved responses are shown together with the true impulse response $h(t)$ in Fig. 4. No visible difference can be appreciated between $h_{1.5}^4$ and the exact solution. Finally, the amplitude of the instantaneous difference $|h(t) - h_{1.5}^4(t)|$ versus time is shown in Fig. 5. As expected, the instantaneous error is high during the early transient and then rapidly decreases.

The above example highlights the fact that, to retrieve the impulse response with an error lower than a few percent, the bandwidth of the Gaussian input has to be so large as to include most of the response spectrum. A "rule of thumb" for the choice of a set of parameters for the impulse response retrieval via FDTD and ME deconvolution may be the following. Let ω_M be the highest frequency to be computed. First, the FDTD mesh size is

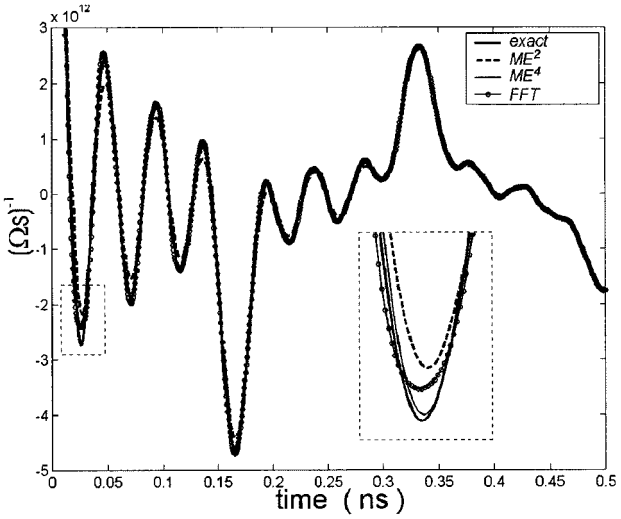

Fig. 4. Retrieved impulse $h\Delta t$ ($\Delta t = 0.6$ ns) response for $\omega_G = 1.5\ \omega_M$.

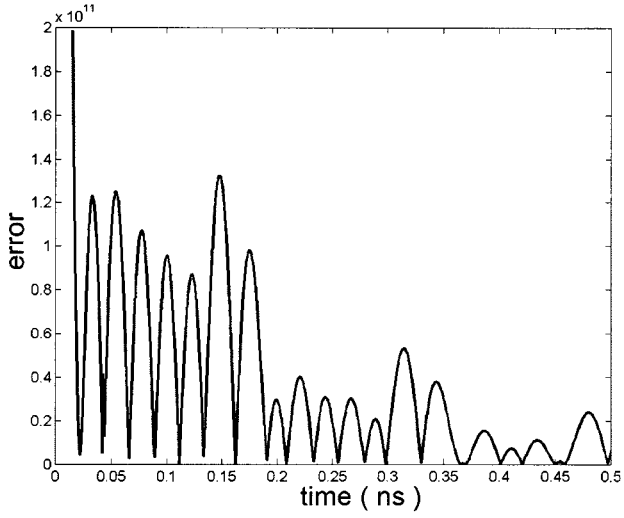

Fig. 5. Instantaneous error $|h(t) - h^4_{1.5}(t)|$ for moment-method deconvolution and the circuit in Fig. 1.

chosen so that $\omega_{\max}^{\mathrm{FDTD}} > r\omega_M$. The Gaussian-pulse parameters are such that its 10% amplitude upper frequency ω_G then lies in the range $[r\omega_M, \omega_{\max}^{\mathrm{FDTD}}]$ with $r \approx 1.5$.

B. Numerical Complexity

The ME method is computationally more efficient than the deconvolution procedure, which involves the Fourier transform. Since additions are usually much faster than multiplications, the numerical complexity of the two methods will be compared in terms of multiplications. For the Fourier-based deconvolutions (2), the FDTD response is first transformed to the frequency domain, then the transform is divided by the spectrum of the input signal, and finally, an inverse Fourier transform is performed. If the response $y_n(t)$ is a vector of N_s time samples, an FFT requires $(1/2)N_s \log_2 N_s$ multiplications [19]. Therefore, the overall Fourier-based deconvolution involves a numerical complexity $O_{\mathrm{FFT}}(Ns) = N_s \log_2 N_s + N_s$.

The ME deconvolution requires the computation of time derivatives, which are numerically evaluated as central differences. Therefore, it is easy to prove that the numerical complexity for an N-order truncated formula is

$$O_{\mathrm{ME^N}}(N_s) = N \cdot N_s. \tag{13}$$

$O_{\mathrm{ME^N}}$ increases linearly with both the truncation order N and the response length N_s. When a Gaussian or a derivated Gaussian pulse is used as input signal, the complexities of the second- and fourth-order deconvolutions are $O_{\mathrm{ME^2}}(N_s) = 2N_s$ and $O_{\mathrm{ME^4}}(N_s) = 3N_s$, respectively. A comparison between complexities is presented in Fig. 6. It can be observed that the number of multiplications required by the ME deconvolution is always lower. Therefore, a computational saving of about one order of magnitude can be achieved when N_s exceeds 1000, as is the case in FDTD simulations.

For the numerical example in Section IV, the number of multiplications for second-order ME, fourth-order ME and FFT deconvolutions were 16.384, 24.576, and 114.688, respectively.

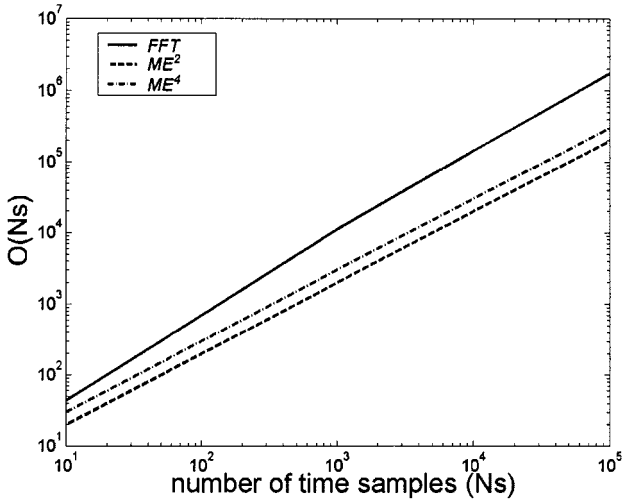

Fig. 6. Numerical complexity of the direct/inverse Fourier transforms and ME method with second- and fourth-order truncation versus the number of time samples.

V. Application to Microwave Devices

A numerical analysis has been carried out for two microwave devices: a multilayer patch antenna (one-port device) and a microstrip low-pass filter (two-port device). The computer program BEST [20] was used for FDTD computation.

A. Patch Antenna

A coaxially fed stacked patch antenna (Fig. 7) was modeled by means of a nonuniform grid with cell size 0.9 mm $\leq \Delta x, \Delta y \leq$ 1.8 mm and 0.3 mm $\leq \Delta z \leq$ 1 mm and time step $\Delta t = 0.78$ ps. The transition between coaxial cable and ground plane was modeled as a real voltage generator [21] with a series lumped resistor $R_0 = 50\ \Omega$, which is equal to the cable resistance. The grid was terminated by six-cell perfectly matched layer (PML) absorbing boundary conditions. The time waveform $v_0(t)$ of the voltage generator was a derivated Gaussian pulse with bandwidth (1.7 GHz, 10 GHz), which is large enough to include the first antenna resonances for standard operations (2.4 GHz to 3.4 GHz).

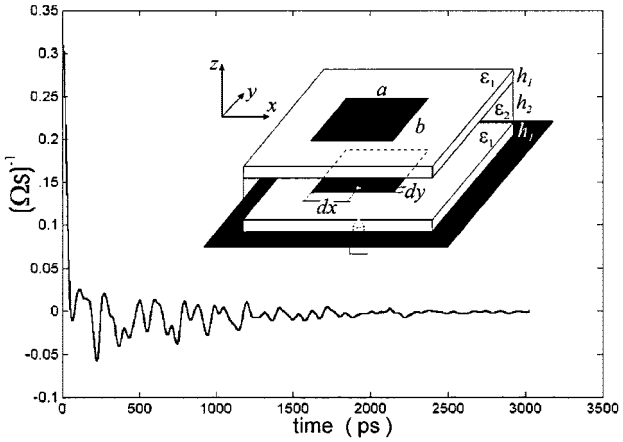

Fig. 7. Current impulse response $h\Delta t$ ($\Delta t = 0.78$ ps) of a stacked patch antenna ($a = 41$ mm, $b = 33.2$ mm, $d_x = 20.9$ mm, $d_y = 5$ mm, $l_1 = 1.57$ mm, $h_2 = 5.4$ mm, $\varepsilon_1 = 2.2, \varepsilon_2 = 1$) at the coax/ground plane transition.

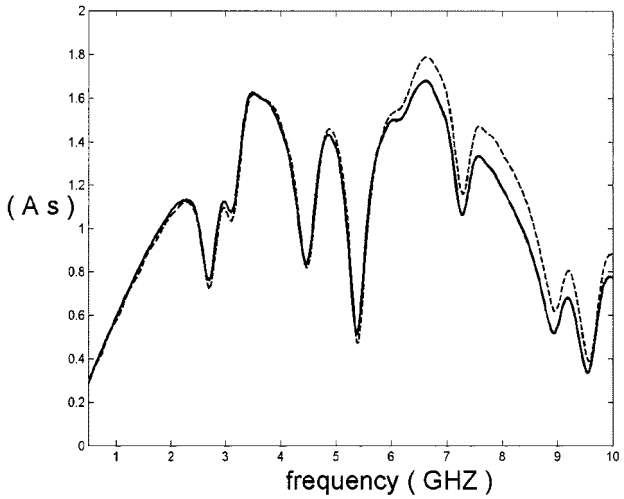

Fig. 9. Fourier transforms of the currents of Fig. 8.

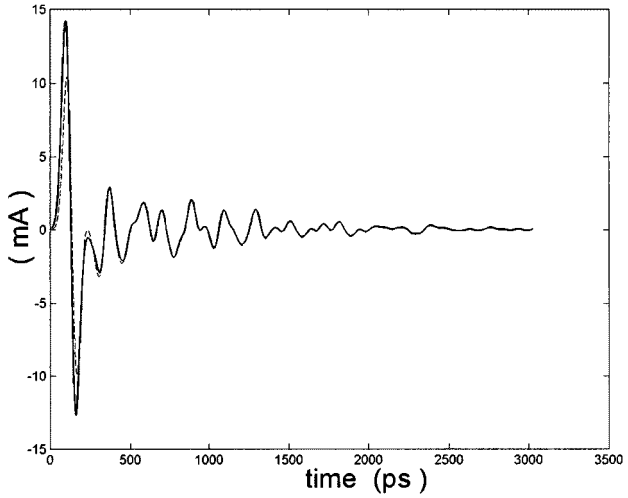

Fig. 8. FDTD-computed current (continuous line) at the coax/ground-plane transition for the antenna in Fig. 7 and the convolution (dashed line) of the test signal with the impulse response deconvolved by the present method.

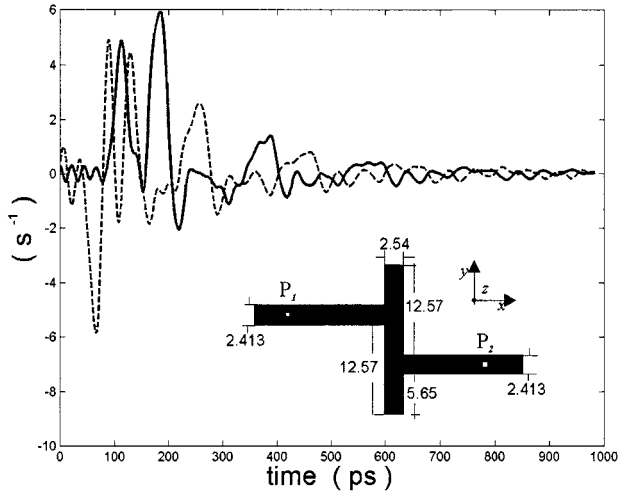

Fig. 10. Planar low-pass filter (size in millimeters) and impulse responses $h_{11}\Delta t$ (dashed line) and $h_{21}\Delta t$ (continuous line) versus time by the FDTD/ME method ($\Delta t = 0.2$ ps).

This structure can be considered as a one-port device. The output observable is the current $i(t)$ at the source point. The current $i(t)$ is evaluated as magnetic field line integral around the excitation point. The impulse response $h(t)$ is defined as the inverse Fourier transform of the input admittance

$$h(t) = \mathcal{F}^{-1}\left[\frac{I(\omega)}{V_0(\omega)}\right] \tag{14}$$

where $V_0(\omega) = \mathcal{F}[v_0(t)]$ and $I(\omega) = \mathcal{F}[i(t)]$.

To lower the high-frequency numerical noise on the FDTD solution, $i(t)$ was low-pass filtered (15-GHz cutoff frequency) before the numerical computation of the second and fourth derivatives of $i(t)$ in (8). The impulse response, computed by ME^4 deconvolution, is shown in Fig. 7. The convolution $v_0 * h(t) = \bar{i}(t)$ was computed and compared with $i(t)$ (Fig. 8) for accuracy evaluation. Full agreement can be observed and the rms error $\delta(i, \bar{i})$ is less than 7%. For completeness, the Fourier transforms of the time signals of Fig. 8 are shown in Fig. 9. A good agreement can be appreciated up to 6 GHz, while the low-pass effect of the proposed ME-deconvolution is responsible for the worsening at higher frequencies.

B. Microstrip Filter

A planar low-pass filter [22] on a 0.794-mm substrate (Fig. 10) with 2.2 permittivity, was meshed on a nonuniform grid with cell sizes 0.3 mm $\leq \Delta x, \Delta y \leq 1$ mm and 0.1 mm $\leq \Delta z \leq 0.5$ mm and time step $\Delta t = 0.23$ ps. The computation domain was truncated by six-cell PML absorbing boundary conditions. The source was modeled as a Huygens-injector template [6] exciting a y^+-directed quasi-TEM mode [Gaussian-pulse bandwidth (0, 27 GHz)]. The structure is a two-port symmetric device. The input waveform is the voltage $v_0(t)$ computed as the line integral of the incident electric field at port P_1 from the ground plane to the microstrip. The output signals are the amplitudes $v_{r,1}(t)$ and $v_{r,2}(t)$ of the outgoing modes from ports P_1 and P_2, respectively, defined as line integrals in the same way. Therefore, the impulse responses are

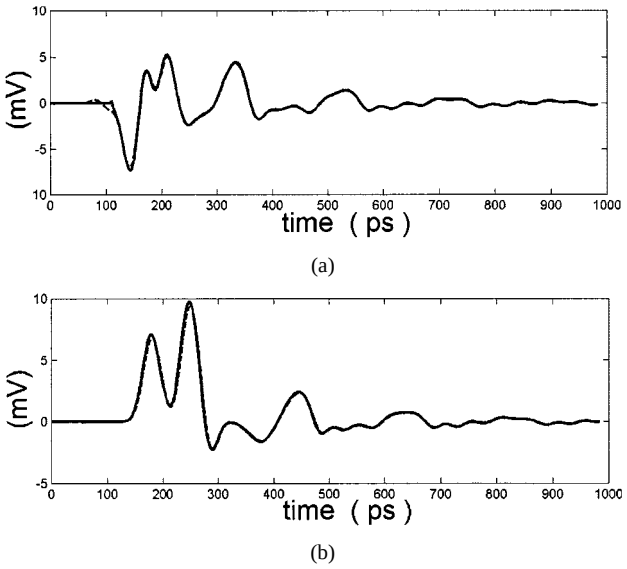

Fig. 11. FDTD-computed outgoing voltages (continuous lines) at: (a) port P_1 and (b) P_2 and the corresponding convolution (dashed lines) of the input Gaussian pulse and the numerical impulse responses h_{11} and h_{21}.

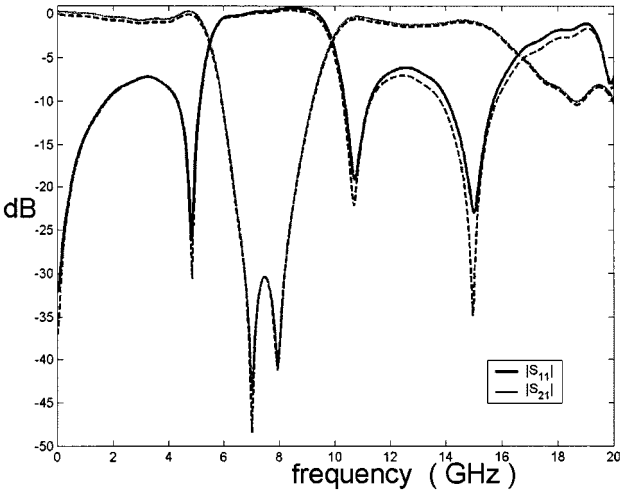

Fig. 12. Frequency-domain scattering parameters S_{11} and S_{21} computed as ratio of transforms (continuous lines) and as Fourier transform (dashed lines) of the impulse responses retrieved by the FDTD–ME method.

the reflection coefficients $h_{11}(t) = h_{22}(t)$ and the transmission coefficients $h_{12}(t) = h_{21}(t)$ defined as

$$v_{r,1}(t) = h_{11} * v_0(t) \tag{15a}$$

$$v_{r,2}(t) = h_{21} * v_0(t). \tag{15b}$$

A time-domain device macromodel can, therefore, be obtained from data computed via a single FDTD run.

Low-pass filtering (20-GHz cutoff frequency) is applied to the output signals before evaluation of derivatives. The computed impulse responses by ME^4 deconvolution are shown in Fig. 10. The convolutions $\overline{v}_{r,1}(t)$ and $\overline{v}_{r,2}(t)$ of the impulse responses and the input voltage are plotted in Fig. 11 for comparison with $v_{r,1}(t)$ and $v_{r,2}(t)$, respectively. The diagrams are indistinguishable almost everywhere and both the rms errors were less than 4%. It is useful to show the scattering parameters in the frequency domain (Fig. 12) as the direct Fourier transform of the FDTD–ME computed impulse responses and as the ratios between the spectra of the reflected voltages $\mathcal{F}[v_{r,i}]_{i=1,2}$ and the input voltage $\mathcal{F}[v_o]$. The low-pass filter performance can be seen in the sharp S_{21} rolloff beginning approximately at 5 GHz, as predicted in [22]. An excellent agreement for both S_{11} and S_{21} parameters can be appreciated at frequencies within the filter bandwidth.

VI. Conclusion

In order to achieve a time-domain macromodel of a microwave device, the impulse response computation by FDTD data processing has been considered in this paper. With reference to Gaussian and derivated-Gaussian input waveforms, a simple time-domain deconvolution algorithm has been proposed. The deconvolution is based on a truncated ME of the input waveform spectrum. The accuracy of the method has been shown to depend on both the truncation order and the input bandwidth. A numerical analysis has been carried out to show that accurate deconvolutions (preserving the accuracy of the FDTD response) can be obtained by means of a fourth-order ME if the input upper frequency is from 1 to 1.5 the response upper frequency. The proposed method was shown to be more accurate and of an order of magnitude computationally more efficient than the FFT-based deconvolution.

References

[1] T. W. Huang, B. Housmand, and T. Itoh, "The implementation of time-domain diakoptics in the FDTD method," *IEEE Trans. Microwave Theory Tech.*, vol. MTT-43, pp. 2149–2155, Nov. 1995.

[2] S. H. Hammadi and S. M. El-Ghazaly, "Extending FDTD/convolution techniques to 3D microwave structures," in *Proc. IEEE AP-S Symp. Dig.*, Seattle, WA, July 1994, pp. 2180–2183.

[3] C. E. Baum, "Toward an engineering theory of electromagnetic scattering: The singularity and eigenmode expansion methods," in *Electromagnetic Scattering*, P. L. E. Uslenghi, Ed. New York: Academic, 1978, pp. 619–651.

[4] W. T. Beyene and J. E. Schutt-Ainè, "Integrating data obtained from electromagnetic field analysis into circuit simulations," in *13th Annu. Rev. Progress Appl. Comput. Electromag.*, vol. 1, 1997, pp. 156–163.

[5] Y. Chen, P. Harms, R. Mittra, and W. Beyene, "Analysis of complex electronic packages with the use of using the FDTD/touchstone hybrid technique," *Microwave Opt. Technol. Lett.*, vol. 12, pp. 313–315, June 1996.

[6] A. Taflove, *Advances in Computational Electromagnetics: The Finite Difference Method*. Norwood, MA: Artech House, 1998.

[7] M. A. Schamberger, S. Kosanovich, and R. Mittra, "Parameter extraction and correction for transmission lines and discontinuities using the finite-difference time-domain method," *IEEE Trans. Microwave Theory Tech.*, vol. 44, pp. 919–925, June 1996.

[8] M. Chen, B. Houshmand, and T. Itoh, "FDTD analysis of a metal-strip-loaded dielectric leaky-wave antenna," *IEEE Trans. Antennas Propagat.*, vol. 45, pp. 1294–1301, Aug. 1997.

[9] M. Fujii, H. Murase, and S. Kobayashi, "FDTD modeling of switching noise in multi-layered digital circuits with CMOS inverters and passive lumped elements," in *IEEE MTT-S Int. Microwave Symp. Dig.*, vol. 3, San Francisco, CA, 1996, pp. 1787–1790.

[10] P. Ciampolini, P. Mezzanotte, L. Roselli, and R. Sorrentino, "Accurate and efficient circuit simulation with lumped-element FDTD technique," *IEEE Trans. Microwave Theory Tech.*, vol. 44, pp. 2207–2215, Dec. 1996.

[11] G. Marrocco and F. Bardati, "FDTD computation of a microwave device impulse response," *Electron. Lett.*, vol. 35, no. 3, pp. 223–224, 1999.

[12] P. G. Petropoulos, "Phase error analysis control for FD-TD methods of second and fourth order accuracy," *IEEE Trans. Antennas Propagat.*, vol. 42, pp. 859–862, June 1994.

[13] A. C. Cangellaris and D. B. Wright, "Analysis of the numerical error caused by the stair-stepped approximation of a conducting boundary in FDTD simulations of electromagnetic phenomena," *IEEE Trans. Antennas Propagat.*, vol. 39, pp. 1518–1525, Oct. 1991.

[14] N. V. Kantartzis and T. D. Tsiboukis, "A comparative study of the Berenger perfectly matched layer, the superabsorption technique and several higher-order ABC's for the FDTD algorithm in two and three dimensional problems," *IEEE Trans. Magn.*, vol. 33, pp. 1460–1463, 1997.
[15] J. Rahman and T. Sarkar, "Deconvolution and total lest squares in finding the impulse response of an electromagnetic system from measured data," *IEEE Trans. Antennas Propagat.*, vol. 43, pp. 416–421, Apr. 1995.
[16] A. J. Poggio, M. L. Van Blaricum, E. K. Miller, and R. Mittra, "Evaluation of a processing technique for transient data," *IEEE Trans. Antennas Propagat.*, vol. AP-26, pp. 165–173, Jan. 1978.
[17] A. Papoulis, "Approximation of point spread for deconvolution," *J. Opt. Soc. Amer.*, vol. 62, pp. 77–80, Jan. 1972.
[18] G. Talenti, "Recovering a function from a finite number of moments," *Inverse Problems*, vol. 3, pp. 501–517, 1987.
[19] A. Papoulis, *Signal Analysis*. New York: McGraw-Hill, 1977, pp. 82–84.
[20] G. Marrocco and F. Bardati, "BEST: A finite difference simulator for time electromagnetcs," *J. Simulation Practice Theory*, no. 7, pp. 279–293, 1999.
[21] R. J. Luebbers and H. S. Langdon, "A simple feed model that reduces time steps needed for FDTD antenna and microstrip calculation," *IEEE Trans. Antennas Propagat.*, vol. 44, pp. 1000–1005, July 1996.
[22] D. Sheen, S. Ali, M. Abouzahra, and J. A. Kong, "Application of the three dimensional finite difference time domain method to the analysis of planar microstrip circuits," *IEEE Trans. Microwave Theory Tech.*, vol. 38, pp. 849–856, July 1990.

Gaetano Marrocco (S'96–M'98) was born in Teramo, Italy, in 1969. He received the Electronic Engineering degree and Ph.D. degree in electromagnetics from the University of L'Aquila, L'Aquila, Italy, in 1994 and 1998, respectively.

In the summer of 1994, he was with the University of Illinois at Urbana-Champaign. In the autumn of 1999, he was a Visiting Researcher at the Imperial College, London, U.K. In 1997, he became a Researcher and Assistant Professor at the University of Rome "Tor Vergata," Rome, Italy, where he currently teaches antenna design. As a consultant, he was involved in several space and avionic programs at the European Space Agency and Italian Space Agency. His research is mainly devoted to the development and optimization of numerical methods and signal-processing techniques for the time-domain modeling of complex electromagnetic structures in the context of industrial and biological applications.

Fernando Bardati (S'63–M'66), photograph and biography not available at time of publication.